Multiscale analysis of waves reflected by complex interfaces: Basic principles and experiments

Yves Le Gonidec, Dominique Gibert, and Jean-Noël Proust

Géosciences Rennes, Centre National de la Recherche Scientifique, Institut National des Sciences de l'Univers, Université Rennes 1, France

Received 7 May 2001; revised 9 March 2002; accepted 14 March 2002; published 13 September 2002.

[1] This paper considers the reflection of waves by multiscale interfaces in the framework of the wavelet transform. First, we show how the wavelet transform is efficient to detect and characterize abrupt changes present in a signal. Locally homogeneous abrupt changes have conspicuous cone-like signatures in the wavelet transform from which their regularity may be obtained. Multiscale clusters of nearby singularities produce a hierarchical arrangement of conical patterns where the multiscale structure of the cluster may be identified. Second, the wavelet response is introduced as a natural extension of the wavelet transform when the signal to be analyzed (i.e., the velocity structure of the medium) can only be remotely probed by propagating wavelets into the medium instead of being directly convolved as in the wavelet transform. The reflected waves produced by the incident wavelets onto the reflectors present in the medium constitute the wavelet response. We show that both transforms are equivalent when multiple scattering is neglected and that cone-like features and ridge functions can be recognized in the wavelet response as well. Experimental applications of the acoustical wavelet response show how useful information can be obtained about remote multiscale reflectors. A first experiment implements the synthetic cases discussed before and concerns the characterization of planar reflectors with finite thicknesses. Another experiment concerns the multiscale characterization of a complex interface constituted by the surface of a layer of monodisperse glass beads immersed in water. *INDEX TERMS:* 7203 Seismology: Body wave propagation; 0935 Exploration Geophysics: Seismic methods (3025); 0669 Electromagnetics: Scattering and diffraction; 5102 Physical Properties of Rocks: Acoustic properties; 5144 Physical Properties of Rocks: Wave attenuation; *KEYWORDS:* multiple scattering, random media, reflectivity, effective media

Citation: Le Gonidec, Y., D. Gibert, and J.-N. Proust , Multiscale analysis of waves reflected by complex interfaces: Basic principles and experiments, *J. Geophys. Res.*, *107*(B9), 2184, doi:10.1029/2001JB000558, 2002.

1. Introduction

[2] A basic concept of seismic reflection is that the geological structures are a merging of homogeneous blocks or layers separated by sharp interfaces where the physical properties of rocks (density, wave velocity) vary abruptly and where reflected and refracted waves appear [e.g., *Claerbout*, 1976; *Bleistein*, 1987; *Dobrin*, 1988; *Henry*, 1997]. Although this model has proved successful in numerous situations, it has long been recognized that the sharp interface concept is not appropriate in many instances where the transitions between layers appear much more complex than the ideal step model. This may be observed in Figure 1a, which represents the compressional velocity of sedimentary rocks measured along a core. Although distinct geological units may be recognized by an expert visual inspection of the core (Figure 1b), the corresponding velocity changes are far from the step-like model in most cases. However, despite the complexity of the velocity profile, the corresponding seismic data show clear reflected waves associated with some of the identified geological interfaces (Figure 1c). This indicates that the seismic waves are able to filter out the small-scale complexity of the velocity variations and to behave as if sharp interfaces representing the coarse-grained structure of the geological layers actually existed underground. As can be observed in the example of Figure 1, this behavior of the waves is not a systematic one, and the correspondence between the geologically recognized main interfaces and the seismic reflectors is not a one-to-one correspondence.

[3] The multiscale variability of the physical properties of the rocks illustrated in Figure 1a has often been argued to reflect the fractal nature of the geological structure of the Earth [*Walden and Hosken*, 1986; *Herrmann*, 1994; *Marsan and Bean*, 1999], and motivated numerous studies devoted to wave propagation in random media [e.g., *Sheng et al.*, 1986, 1989; *Burridge et al.*, 1988; *Gibson and Levander*, 1990; *Scales*, 1993]. In such studies, the geophysical signals

0148-0227/02/2001JB000558$09.00

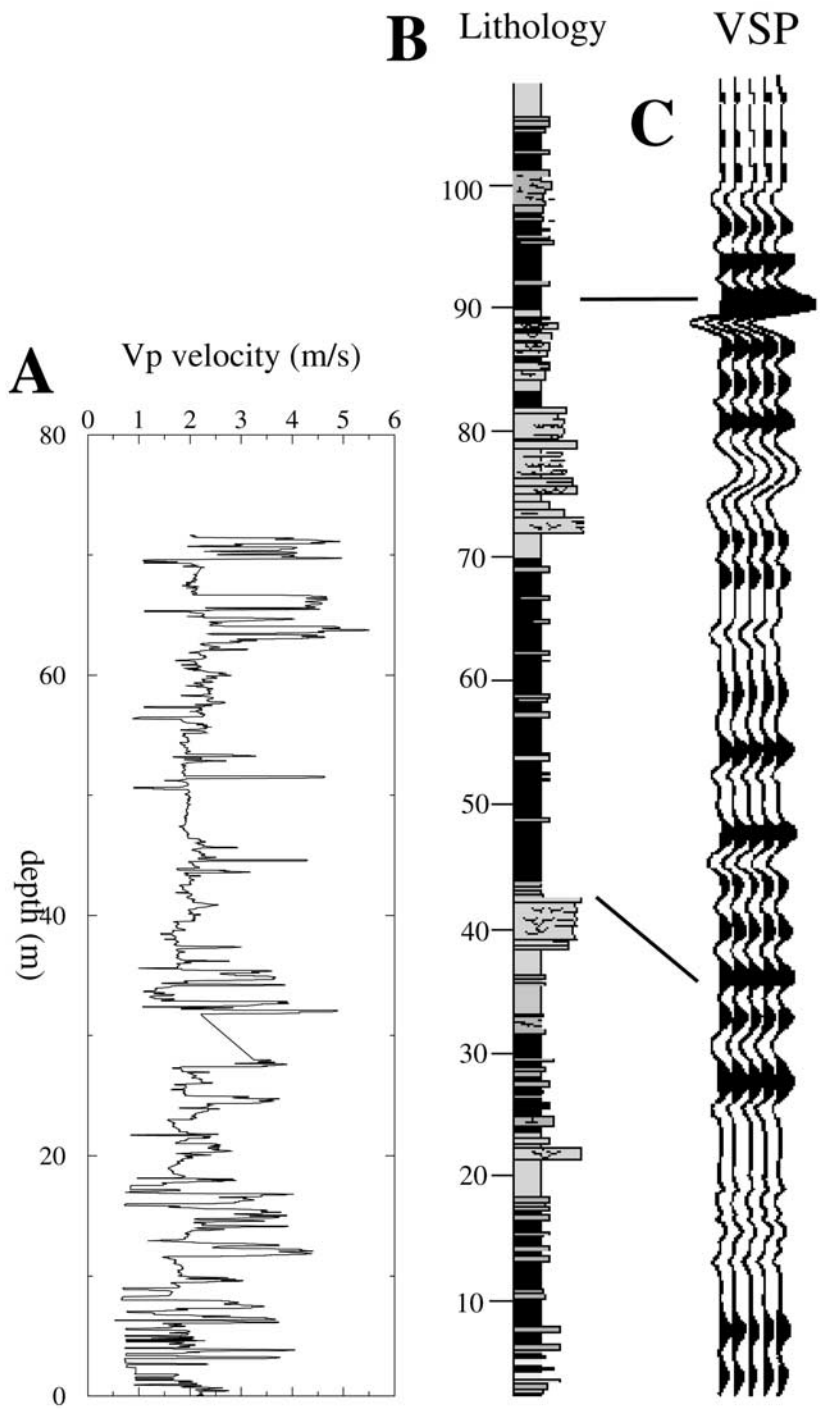

Figure 1. (a) Compressional velocity measured along a sedimentary core. (b) Interpreted geological log. (c) Seismic data obtained from a vertical seismic profile.

(e.g., diagraphy logs, seismic signals) are seen as statistical quantities where the initial concept of isolated step-like interface disappears in favor of ensemble-averaged statistical attributes like correlation length, fractal dimension, coda extinction time, etc. Although useful in several instances, the statistical approach eliminates the deterministic notion of reflector which, however, practically agrees with the reflected waves visible in most seismic data. The intricate and puzzling relationships between the geologically interpreted log, the core velocity profile, and the seismic data rise several fundamental and long-standing questions concerning the information content brought by the seismic waves about the geological structures [*Widess*, 1973; *Banik et al.*, 1985; *Burridge et al.*, 1988]. In particular, the filtering effects of the waves need to be quantified, and it is interesting to evaluate the influence of the small-scale

features of the medium onto the long-wavelength waves whose propagation may be strongly altered through multiple scattering and interference phenomena. A related question concerns the extent to which long-wavelength waves are able to carry information concerning small-scale details of the geological layers [e.g., *Widess*, 1973, 1982; *Knapp*, 1990].

[4] In the present paper we present a multiscale approach to analyze the complex (instead of random) structure of reflectors. First, the wavelet transform is used to analyze the local multiscale structure of the variations of the rock properties associated with a reflector. The wavelet analysis is well-suited to characterize the geometry (i.e., the regularity) of the detected abrupt changes and to establish the scale domain where the sharp interface simplification may be defined [e.g., *Alexandrescu et al.*, 1995, 1996]. This analysis also allows identification of the scales where the concept of step-like interface is no longer valid and where the whole complexity of the velocity changes must be considered. From a geometrical point of view, and following *Argoul et al.* [1989], the wavelet transform acts as a mathematical microscope able to give a quantitative measure of the local appearance of a signal at different scales. This is possible because, contrary to the windowed Fourier transform, wavelets are oscillating functions of constant shape whose width narrows as frequency increases. Synthetic examples of increasing complexity are used to illustrate the method. In the second half of the paper, we turn to the reflection of seismic waves by a multiscale interface and introduce the "wavelet response" method. This approach is a natural extension of the wavelet analysis obtained by replacing the convolution operator by the propagator through the complex medium and has been independently used by *Herrmann and Staal* [1996] and *Wapenaar* [1998, 1999] in the case of self-similar (i.e., homogeneous) interfaces. We show that when multiple scattering is neglected, both the wavelet transform and the wavelet response are equivalent. The results obtained with both methods are compared in order to evaluate which amount of information is carried by the waves. These examples reveal that both methods give the same asymptotic results (i.e., at very small and very large scales). In the intermediate-scale range, both methods produce complicated results sometimes impossible to analyze quantitatively. However, the critical scales defined as the ends of the intermediate-scale range remain robust indicators of the scales present in the medium. The paper ends with two experiments made in a water tank. The first one presents the wavelet response of plates with plane parallel faces, and the second experiment concerns the wavelet response of a complex interface represented by the surface of a layer of glass beads.

2. Wavelet Analysis of Multiscale Reflectors

2.1. Wavelet Transform of Homogeneous Functions

[5] In the present paper, the continuous wavelet transform is used to perform a multiscale analysis of complex signals and to give an insight of their hierarchical organization at various scales. We shall write the continuous wavelet transform of a function s as a convolution product,

$$\mathcal{W}[g,s](b,a) \equiv (\mathcal{D}_a g * s)(b), \tag{1}$$

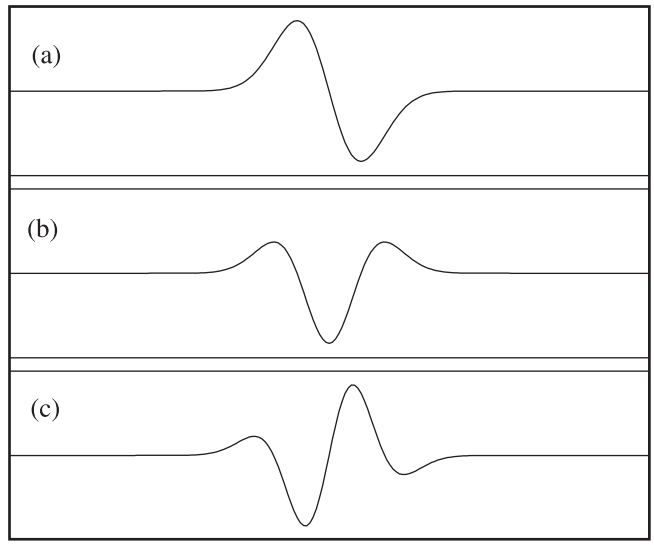

Figure 2. Examples of analyzing wavelets used defined as the (a) first, (b) second, and (c) third derivatives of a Gaussian function. The wavelet (Figure 2b) is also commonly referred to as the "Ricker" wavelet in seismic and as the "Mexican hat" wavelet in the wavelet literature. The main property to be satisfied by a wavelet is to possess a vanishing integral, but depending on its number of vanishing moments, a given wavelet is able to detect singularities up to a maximum homogeneity degree.

where b is the position variable (i.e., space or time), g is the analyzing wavelet, and $\mathcal{D}_a$ is the dilation operator acting as

$$\mathcal{D}_a g(b) \equiv \frac{1}{a} g\left(\frac{b}{a}\right), \tag{2}$$

where the dilation $a > 0$. The analyzing wavelet may be either a real or a complex oscillating localized function (i.e., with a compact or quasi-compact support) with a vanishing integral (Figure 2). The wavelet transform has been introduced in geophysics by *Goupillaud et al.* [1984] and in mathematical physics by *Grossmann and Morlet* [1984]. Among the many nice mathematical properties of the wavelet transform (see, for instance, *Holschneider* [1995] for a general introduction) is its remarkable behavior when the analyzed signal is quasi-homogeneous, i.e., when s may be written as

$$s(b) = s_h(b) + p(b), \tag{3}$$

where $p(b)$ is a polynomial assumed to belong to the null-space of the wavelet transform (i.e., $\mathcal{W}[g, p]\,(b, a) = 0$) and $s_h(b)$ is an homogeneous function which verifies

$$s_h(\lambda b) = \lambda^{\alpha} s_h(b), \tag{4}$$

with α the homogeneity degree. The maximum degree M of the polynomials in the null-space must be smaller than the number of vanishing moments of the analyzing wavelet. For such a quasi-homogeneous function, equation (1) gives [*Grossmann*, 1986; *Grossmann et al.*, 1987]:

$$\mathcal{W}[g,s](\lambda b, \lambda a) = \lambda^{\alpha} \mathcal{W}[g,s](b,a), \tag{5}$$

which means that the whole wavelet transform may be extrapolated over the entire half-space (b, $a > 0$) from the wavelet transform given at a single dilation. The geometrical translation of this property is that the wavelet transform of an homogeneous function has a cone-like structure converging toward the homogeneity center of the analyzed function [*Mallat and Hwang*, 1992]. Also, equation (5) indicates that the magnitude of the wavelet transform taken along any straight line crossing the homogeneity center is a power law of exponent α with respect to the dilation a [*Holschneider*, 1995]. The homogeneity degree α may then simply be recovered by computing the slope of the power law plotted in a log-log diagram. Among the straight lines which can be chosen to obtain the power law, those corresponding to the extrema of the wavelet transform modulus are of particular interest since they have the best signal-to-noise ratio. Following the definition used by *Alexandrescu et al.* [1995, 1996], we shall hereinafter define the ridge function $r_j(a)$ as the absolute value of the wavelet transform taken along a given line of maxima:

$$r_j(a) \equiv \left|\mathcal{W}[g,s]\left(b_{\max,j},a\right)\right|, \tag{6}$$

where $b_{\max,j}(a)$ is the position of the jth extrema of the dilated wavelet $\mathcal{D}_a g$. Another advantage of the ridge functions is that they automatically conform with the conical geometry of the wavelet transform and that its not necessary to a priori know the location of the homogeneity center to find them. This advantage is very useful when studying wavelet transforms of complicated signals.

2.2. Analysis of Isolated Singularities

[6] The theoretical framework presented in section 2.1 is now illustrated through the wavelet analysis of several pure homogeneous singularities aimed at representing ideal interfaces. The first one is the Heaviside or step distribution (bottom part of Figure 3a) which corresponds to $\alpha = 0$ in equation (4) and could represent the ideal sharp transition of petrophysical properties between two homogeneous geological layers. From the seismic point of view, the Heaviside distribution is an ideal diopter where an incident wave is both reflected and transmitted. The modulus of the wavelet transform of the step distribution is shown in Figure 3a and was obtained with the analyzing wavelet shown in Figure 2c. As can be observed, the wavelet transform has a cone-like geometry with lines of maxima converging toward the homogeneity center of the distribution, i.e., where the step occurs (the lines of maxima are not straight lines because of the log scale for the dilation axis). When plotted as a function of dilation in a log-log diagram (Figure 3b), the wavelet transform modulus taken along the lines of maxima (i.e., the ridge functions $r_j(a)$) follows a linear law. In the present instance, the ridges functions are horizontal straight lines in accordance with the theoretical homogeneity degree $\alpha = 0$.

[7] Another singularity of interest is the Dirac δ distribution whose homogeneity $\alpha = -1$ and is aimed at ideally representing an infinitely thin geological layer embedded in a homogeneous medium. As in the previous example, the wavelet transform of this distribution possesses the typical conical geometry (Figure 3c), and the ridge functions also appear as straight lines in a log-log diagram with a slope $\alpha = -1$ (Figure 3d).

[8] The last example considers the wavelet transform of a ramp function with $\alpha = 1$ which may represent a layer with physical properties changing linearly with depth. This may, for instance, be encountered in layers of unconsolidated sediments where the compaction increases with depth (i.e., pressure) and produces velocity and density gradients. The geological interface of interest is located at the top of the layer and corresponds to the transition between the overlying homogeneous layer (e.g., water in marine seismic) and the gradient layer. The wavelet transform of the ramp function has a conical geometry pointing toward this interface (Figure 3e) and possesses two ridge functions with $\alpha = 1$ (Figure 3e).

[9] These examples show how the wavelet transform both automatically detects and characterizes sharp homogeneous changes present in a signal. The homogeneity center at the location of the abrupt change corresponds to the apex of the conical structure of the wavelet transform. The ridge functions $r_j(a)$ taken along the lines of maxima of the wavelet transform modulus appear as straight lines in a log-log diagram with a slope α equals to the homogeneity degree of the singularity. Let us emphasize that α is not necessarily an integer (see *Alexandrescu et al.* [1995, 1996] for further examples) and that the number n of ridge functions associated with a singularity decrease by one each time α increases by one integer value. So, in addition to their slopes α, the number n of ridge functions may be used as a rough indicator of the homogeneity degree. For the analyzing wavelet used in these examples (Figure 2c), $n = 4$ implies $-1 \leq \alpha < 0$, $n = 3$ implies $0 \leq \alpha < 1$, and so on, until $2 \leq \alpha < 3$, where the limit $n = 1$ beyond which no ridge function exists is reached. To detect singularities with $\alpha \geq 3$, an analyzing wavelet with more extrema (i.e., with more vanishing moments) must be used.

2.3. Multiscale Singularities

[10] We now address the case of multiscale singularities, the first one is a window function (Figure 4a) whose width defines a characteristic scale a_c. For dilations $2^2 < a < 2^4$ much smaller than a_c, the wavelet transform of the window (Figure 4a) has two cone-like patterns converging toward the edges of the window. The ridge functions are horizontal in the same dilation range and indicate that the detected singularities are Heaviside-like with $\alpha = 0$ (Figure 4b). For larger dilations, the two cones observed at small dilations merge to form a single complicated pattern with an anastomosis of the ridges functions whose linear behavior disappears in the critical dilation range $2^4 < a < 2^5$ (Figure 4b). At even larger dilations, $a > 2^5$, the ridge functions are again linear with a negative slope $\alpha = -0.7$ indicating that the window begins to approximate a Dirac distribution. The number n of ridge functions varies accordingly with $n = 3$ at small dilations, and $n = 4$ at large ones. Observe that the two ridge functions displayed in Figure 4b have identical shapes (i.e., straight appearance) at both small and large dilations but are very different in the critical dilation range.

[11] A more complicated signal with two characteristic scales is constructed with three nearby Heaviside distributions (Figure 4c). The smallest characteristic scale corresponds to the distance between adjacent steps and the

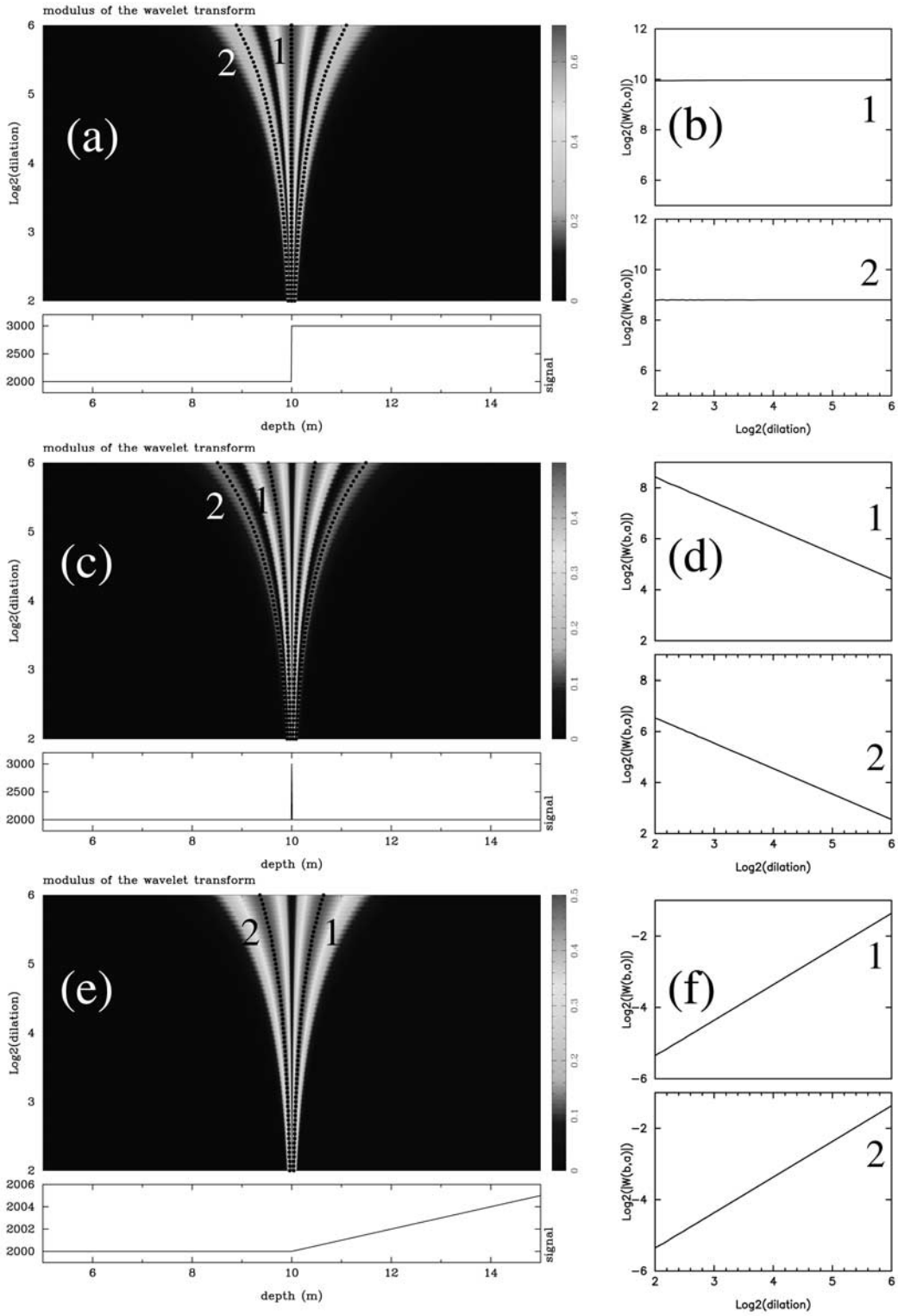

Figure 3. (left) Modulus of the continuous wavelet transforms of (a) a Heaviside distribution, (c) a Dirac distribution, and (e) a ramp function. The analyzing wavelet used to obtain these transforms is shown in Figure 2c. The wavelet transforms display a cone-like structure with a variable number of ridge functions (black dotted lines) converging toward the homogeneity center of the analyzed signal. The color scale is renormalized for each dilation in order to enhance the conical structure of the wavelet transform. (right) The $\log_2$-$\log_2$ plots of the two leftmost ridge functions of each wavelet transform shown on the left. All ridge functions appear as straight lines whose slope α equals the homogeneity degree of the detected singularity: (b) $\alpha = 0$, (d) $\alpha = -1$, and (f) $\alpha = +1$.

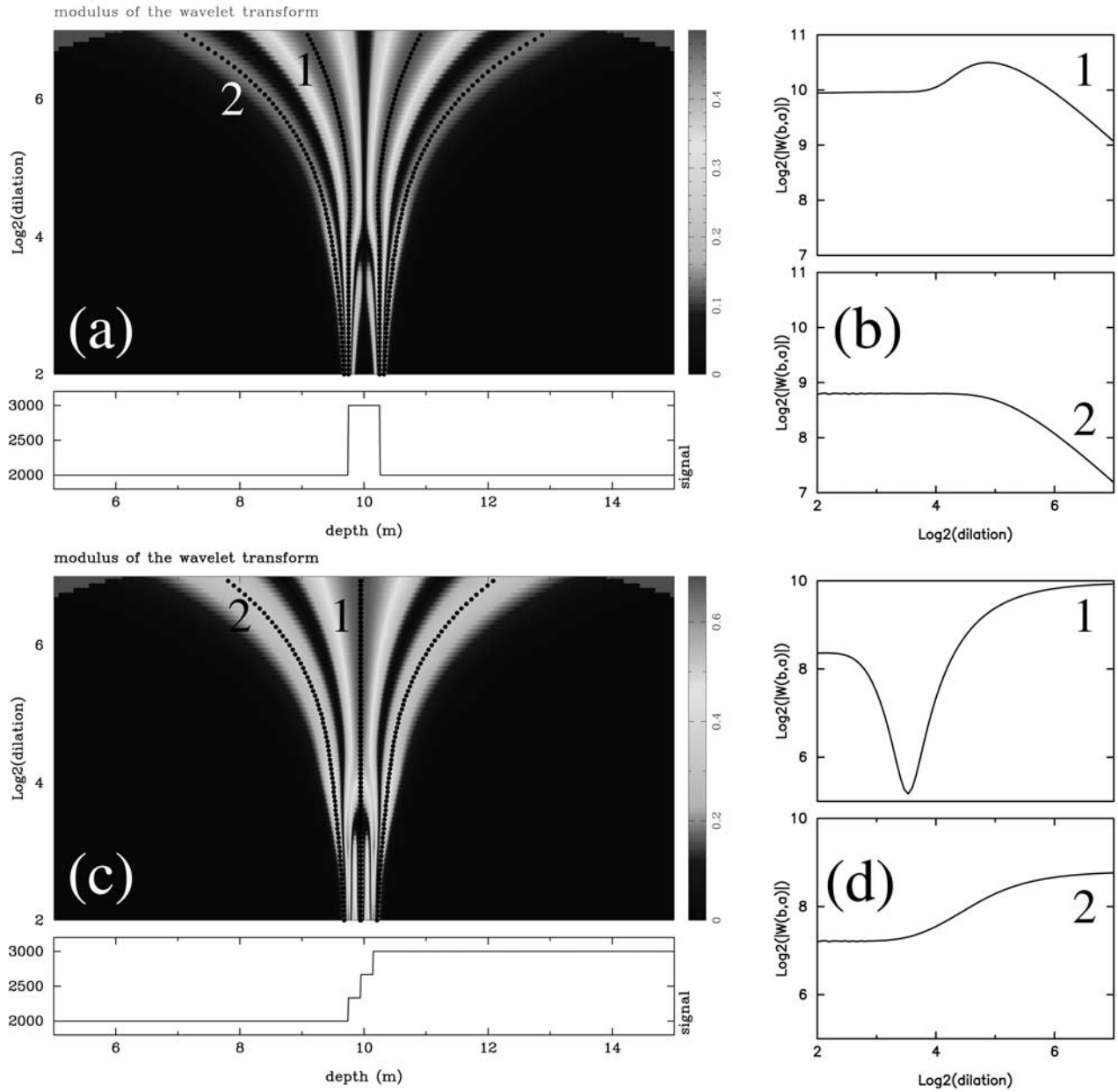

Figure 4. (a) Modulus of the wavelet transform of a window function. At small dilations, the wavelet transform possesses 2 conical structures converging toward the ends of the window and indicating that the window appears as 2 successive singularities. At larger dilations, the wavelet transform displays a unique cone-like feature converging toward the center of the window and more typical of a Dirac distribution. (b) The $\log_2$-$\log_2$ plot of the two leftmost ridge functions of the wavelet transform shown on the left. At small dilations, $a < 2^4$, the ridge functions are horizontal with $\alpha = 0$, and for $a > 2^5$ the slope $\alpha = -0.7$ is more typical of a Dirac-like singularity. (c) Modulus of the wavelet transform of a signal composed of three successive Heaviside distributions. When spanning the whole dilation range $2^2 < a < 2^7$, the wavelet transform displays three, two, and one conical structures indicating that the analyzed signal possesses three scale-dependent appearances. (d) The $\log_2$-$\log_2$ plot of the two leftmost ridge functions of the wavelet transform shown on the left. The ridge function labeled 1 (the leftmost one in the wavelet transform) clearly shows the three scale-dependent appearances suggested by the structure of the wavelet transform. The small-dilation part of this ridge function indicates $\alpha = 0$, the intermediate one indicates $\alpha = 0.8$, and the large one indicates $\alpha = 0$. The intermediate-scale appearance of the signal is not well-captured by the ridge function labeled 2 (the central one in the wavelet transform) because of complicated interferences among the individual conical structures of the wavelet transform. However, this ridge function correctly restores the small- and large-dilation regularities.

largest is defined by the distance separating the two extremal steps. At small dilations $a < 2^3$ the wavelet transform has three cones converging toward the individual Heaviside distributions, and their ridge functions are horizontal (Figure 4d). At larger dilations $2^3 < a < 2^4$ the three cones merge, and the ridge functions are no more linear until the range $2^4 < a < 2^5$ where the extremal ridge functions (the leftmost being labeled 2 in Figure 4d) are linear with a positive slope $\alpha = 0.8$ typical of a ramp-like singularity. For this dilation range the wavelet transform possesses only two cones pointing toward the ends of the global signal indicating that at these scales the signal appears as the sum of 2 successive ramp functions. The central ridge function (labeled 1 in Figure 4d) is more complicated with a wiggly appearance in the $2^3 < a < 2^5$ range. At larger dilations a second transition is encountered for $2^5 < a < 2^6$ where the two cones merge and where all ridge functions are again nonlinear. Finally, at large dilations $a > 2^6$ the wavelet transform reduces to a unique conical feature, and all ridge functions become progressively linear and horizontal with $\alpha = 0.1$ (Figure 4d), indicating that at large scales the signal appears as a Heaviside distribution.

[12] These examples show that the wavelet transform efficiently enhances the information about abrupt changes present in a signal by showing conspicuous cone-like patterns in the wavelet map. At observation scales where the abrupt changes appear homogeneous, the ridge functions follows a power law and varies linearly with respect to the dilation when plotted in a log-log diagram. For clusters of nearby singularities (Figure 4) the wavelet transform possesses a hierarchical arrangement of conical patterns which constitute a mean to probe the multiscale nature of the cluster. This hierarchical arrangement is also present in the ridge functions which appear wiggly with straight segments in dilation ranges where the analyzed signal locally appears homogeneous.

3. Wavelet Response of Multiscale Reflectors

3.1. Definition of the Wavelet Response

[13] We have shown how the wavelet transform may be used to analyze the scale-dependent structure of a multiscale signal. We now examine the possibility to remotely analyze a multiscale reflector by propagating a family of wavelets through the velocity structure. This is done by performing what will hereinafter be referred to as the ''wavelet response'' obtained by recording the reflected wave fields for a family of source wavelets. In accordance with the notations of equation (1) we define the one-dimensional (1-D) wavelet response as

$$\mathcal{R}[g,s](b,a) \equiv \left(\mathcal{D}_a g \bigotimes s\right)(b), \tag{7}$$

where the $\otimes$ represents the 1-D propagation of the dilated wavelet $\mathcal{D}_a g(t)$ through the velocity profile $s(z)$. Physically, the wavelet response represents the reflected time-varying wave field recorded at a given depth z_r, the source wavelet being emitted at depth z_s. Since the wavelet response is the reflected wave field, it is implicitly assumed that both the source and the recording points are located on the same side of the reflector to be probed. Let us emphasize that the position variable b represents the depth in the wavelet transform while it represents the two-way time in the wavelet response. Hence both transforms are not in the same spaces and are not directly comparable.

[14] A link between the wavelet response (7) and the wavelet transform (1) may be established when multiple scattering is neglected. In such a case, it can be shown [e.g., *Gray and Bleistein*, 1986] that the reflected wave field corresponding to a Dirac source equals the reflectivity function $r(t)$ defined by

$$r(t) \equiv \frac{1}{2}\frac{d}{dt}\ln \gamma(t), \tag{8}$$

where the acoustical impedance $\gamma(t) = \rho(t)\, s(t)$ and the correspondence from depth to time is given by

$$t(z) = \int_{z_s}^{z} s^{-1}(\xi)\, d\xi + \int_{z_r}^{z} s^{-1}(\xi)\, d\xi. \tag{9}$$

If we further assume that the density ρ is a constant, and use equation (9) to flip from temporal to spatial derivative, we get from equation (8)

$$r(t) = \frac{1}{4}\frac{d}{dz} s[z(t)]. \tag{10}$$

If the source signal is a dilated wavelet $\mathcal{D}_a g(t)$, the wave field (i.e., the wavelet response) is obtained through a convolution,

$$\mathcal{R}[g,s](b,a) \equiv \left(\mathcal{D}_a g * \frac{d}{dz} s[z(t)]\right)(b), \tag{11}$$

A comparison of equations (1) and (11) shows that the wavelet response of the velocity profile s is the wavelet transform of the first space derivative of the velocity profile. Let us emphasize that this result is valid only when both multiple scattering and density variations are neglected. If multiple scattering cannot be neglected, the reflected wave field is much more complicated than the reflectivity and huge discrepancies appear between the wavelet transform and the wavelet response.

3.2. Wavelet Response of Isolated Reflectors

[15] We now apply the wavelet response to the Heaviside distribution aimed at representing an ideal velocity jump between two homogeneous half-spaces. In such a situation, no multiple scattering occurs, and this example then corresponds to an ideal case where the wavelet response reduces to the wavelet transform. The wavelet response is shown in Figure 5a, the analyzing wavelet is the one shown in Figure 2b and is the integral of the wavelet used for the wavelet analysis presented in sections 2.2 and 2.3. This choice for the analyzing wavelets has the advantage to produce the same number of ridge functions in both the wavelet transform and the wavelet response and allows an easy comparison between both transforms. Also, in order to obtain the same slope α as for the wavelet transform, each line of the wavelet response has been multiplied by the dilation a. In practice, each horizontal line of the wavelet response map is actually a

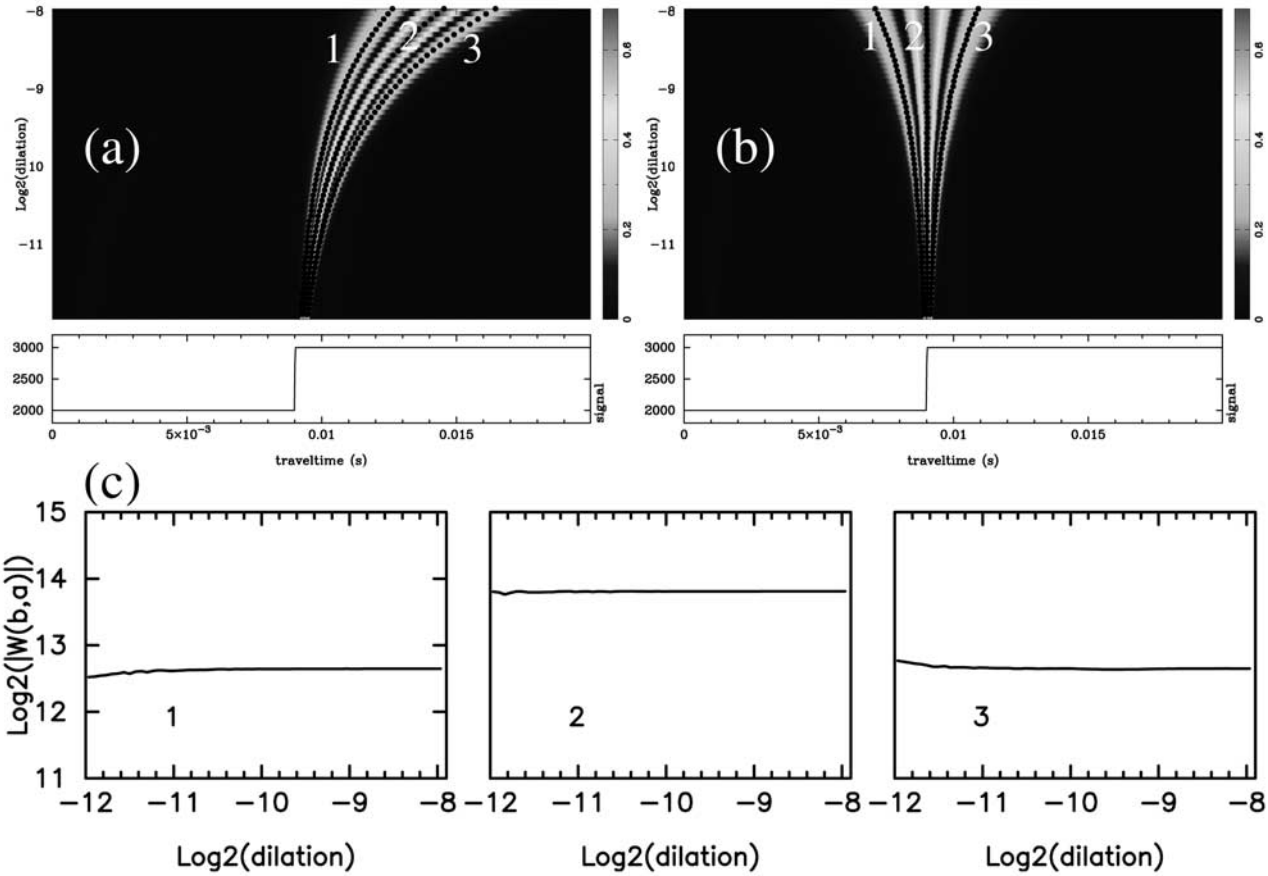

Figure 5. (a) Modulus of the wavelet response of a Heaviside velocity distribution. Each horizontal line of the wavelet response is actually a seismic trace obtained by propagating a wavelet of dilation a and recording its reflections onto the reflectors. In the present instance, the source and the receiver are located at the very left of the signal so that the incident wave field propagates rightward and the reflected wave field propagates leftward. The conical feature located in the middle of the wavelet response corresponds to the waves reflected by the reflector associated with the velocity jump. The wavelet response possesses three ridge functions (black dots in the top panel) which converge toward the homogeneity center of the velocity jump. (b) Noncausal representation of the wavelet response shown on the left obtained by shifting each trace by the half duration of the source wavelet. (c) The $\log_2$-$\log_2$ plot of the ridge functions of the wavelet responses.

seismic trace obtained by propagating (using a finite difference method) a wavelet of dilation a and recording the corresponding reflected response. The whole wavelet response is then a stack of such seismic traces arranged with increasing dilation in order to obtain a picture similar to a wavelet transform. All wavelet responses shown in this paper are such that the source and the receiver points are located at the same place (i.e., $z_r = z_s$). The stacked traces form a conical feature identical to the ones obtained with the wavelet transform and corresponding to the waves reflected by the reflector associated with the velocity jump. One can observe that the conical pattern associated with the velocity jump counts three ridge functions as observed in the wavelet transform, a correspondence due to the careful choice of the analyzing wavelet. The inclination of the cone is caused by the fact that the source wavelet is causal, contrary to the wavelets used in the wavelet transform. This may be a posteriori corrected by shifting each trace by the half duration of the source. The resulting noncausal representation of the wavelet response looks more similar to the wavelet transforms (Figure 5b). The ridge functions plotted in a log-log diagram (Figure 5c) appear horizontal in accordance with the regularity $\alpha = 0$ of the Heaviside distribution.

3.3. Wavelet Response of Multiscale Reflectors

[16] We begin with the window function whose wavelet response (Figure 6a) has a conical structure with four ridge functions at large dilations and typical of a Dirac distribution (compare with Figure 3c). At small dilations, and as observed in the wavelet transform of the window (Figure 4a), the main cone of the wavelet response splits into two cones pointing toward the edges of the window and counting three ridge functions typical of an Heaviside distribution (compare with Figure 3a). This twofold appearance of the window also exists in the log-log plots of the ridge functions (Figure 6b), which are flat with $\alpha \simeq 0$ at small dilations and monotonically decrease with $\alpha \simeq -0.85$ at

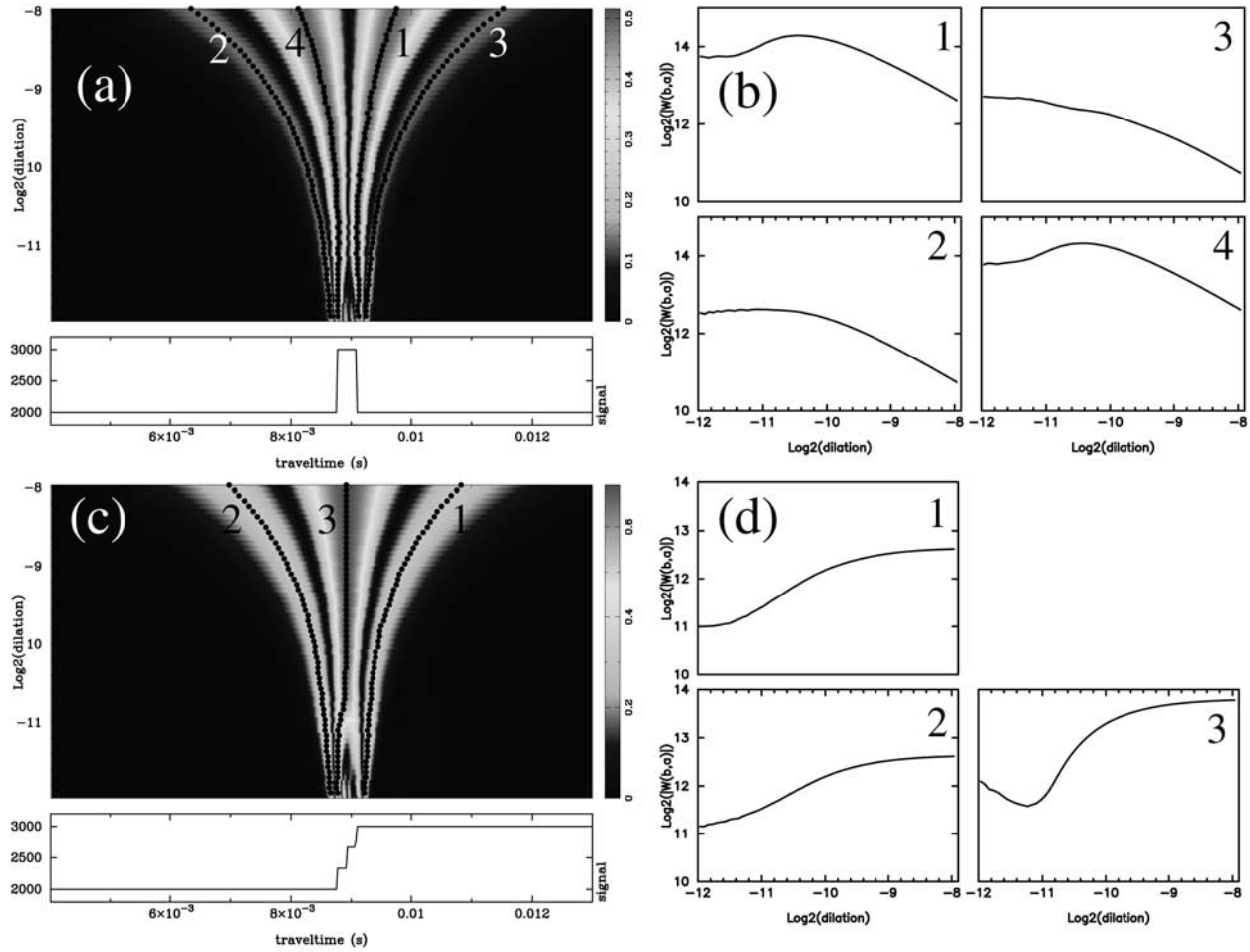

Figure 6. (a) Modulus of the wavelet response of a window function. The analyzing wavelet is the one shown in Figure 2b. At large dilations the wavelet response possesses four ridge functions typical of a Dirac distribution. At small dilations, the main conical pattern is split into two small cones pointing toward the edges of the window and counting three ridge functions typical of an Heaviside distribution. (b) The $\log_2$-$\log_2$ plot of the main four ridge functions of the wavelet response displayed in Figure 6a. (c) Modulus of the wavelet response of a signal composed of three nearby Heaviside steps. At large dilations the wavelet response possesses a single cone with three ridge functions typical of a Heaviside distribution. At medium dilations the single main cone is split into two cones with two ridge functions each, typical of a ramp-like singularity. At small dilations the conical pattern becomes more complicated with no simple structure. (d) the $\log_2$-$\log_2$ plot of the main three ridge functions of the wavelet response displayed in Figure 6c.

large dilations. In the intermediate dilation range the ridge functions do not display a well-defined slope because of complicated interference phenomena between the two subcones. The wavelet response then allows quantitative assessment of the multiscale nature of the reflector by indicating that for high-frequency (i.e., small dilations) wavelets the reflector appears as two separated step-like reflectors while at low frequency (i.e., large dilations) the same structure appears as a Dirac-like reflector. As for the wavelet transform, the outer ridge functions located on the edges of the cone (i.e., lines 2 and 3) are less wiggly than the inner ridges functions (i.e., lines 1 and 4), which are more affected by interference phenomena. Let us remark that contrarily to the wavelet transform which is symmetrical, the ridge functions of the wavelet response are nonsymmetrical (i.e., lines 2 and 4 differ from lines 1 and 3, respectively) because the wavelet response is polarized (i.e., the reflected waves forming the wavelet response are coming from the right since the source and the receiver are located at the very left of the velocity profile). The corner dilations corresponding to the upper end of the small-dilation range are different for the outer ridges ($a_c = 2^{-11}$) and for the inner ridges ($a_c = 2^{-11.5}$). Since the inner ridges are mostly affected by the internal interference phenomena occurring in the fine structure of the reflector, their corner dilations are a good indicator of the size of the structure. Indeed, the corner wavelength (simply obtained by multiplying the dilation with the velocity in the present paper) corresponding to $a_c = 2^{-11.5}$ is $\lambda = 1$ m which is twice the width of the window reflector used in this example.

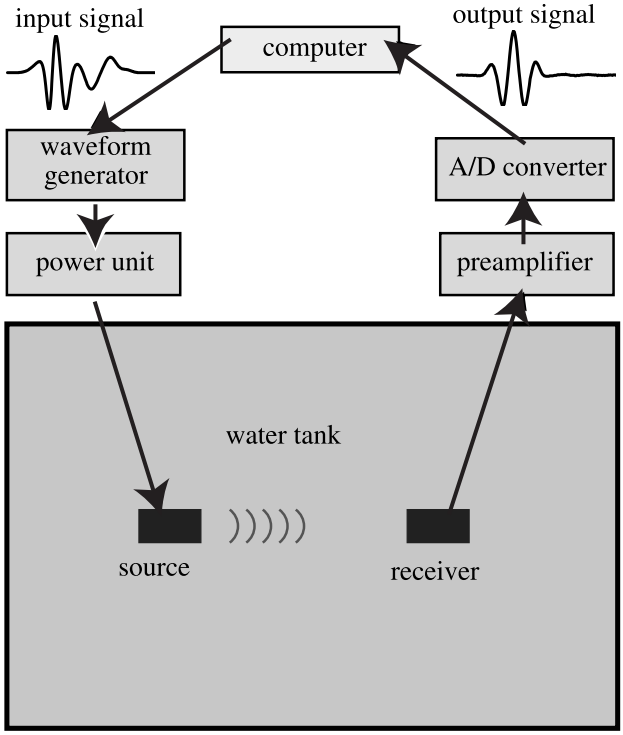

Figure 7. Schematic view of the setup used to construct the experimental wavelet response. A nonlinear inverse method (F. Conil, personal communication, 2002) is used to find the numerical input signal (top left) to send to the arbitrary waveform generator in order to obtain an output signal (top right) equal to a pure wavelet as the one shown in Figure 8.

[17] The second example concerns the cluster of Heaviside velocity jumps already shown in Figure 6c and having two characteristic scales defined by the interval between adjacent steps and by the overall width of the reflector. The large-dilation part $a > 2^{-10.5}$ of the wavelet response is a single cone with three ridge functions typical of a Heaviside distribution. At intermediate dilations $a \simeq 2^{-11}$ this cone is split into two cones with two ridges each, and at smaller dilations $a < 2^{-11.5}$ these two cones disappear while more ridges appear. This threefold appearance of the wavelet response is present in the log-log plots of the inner ridge function (labeled 3 in Figure 6d). The outer ridges of the main cone (ridges 1 and 2 in Figure 6d) are less affected by the interference phenomena and display the simplest behavior with a flat appearance at small ($a < 2^{-11.5}$) and large ($a > 2^{-9.5}$) dilations and a positive slope at intermediate dilations. This is coherent with the wavelet analysis of the same signal (Figure 4d) which indicates that this multiscale signal has an Heaviside-like appearance at small and large dilations and a ramp-like behavior at intermediate dilations. The inner ridge function provides a corner dilation $a_c = 2^{-11.5}$ which corresponds to a corner wavelength $\lambda_c = 1$ m, indicating a width of the reflector equals to half a meter.

[18] The wavelet response of the two multiscale synthetic signals considered in this section is coherent with the results obtained with the wavelet analysis of the same signals. In particular, we observe that the asymptotic appearance of the signals at very small and very large dilations is the same for both the wavelet transform and the wavelet response, indicating that neglecting multiple scattering seems valid and that the convolution approximation (11) of the wavelet response is acceptable. The ridge functions extracted from the wavelet response look very similar to the one obtained with the wavelet transform with second-order discrepancies due to the nonsymmetrical nature of the wavelet response and to interference phenomena occurring at medium dilations. The wavelet response then constitutes a tool to remotely probe both the coarse and the fine structure of a reflector. The slopes derived from the outer ridge functions are most useful to infer for the fine-scale and global-scale appearances of the reflector, and the corner dilations identified in the log–log plots of the inner ridge functions provide information about the width of the reflector.

4. Acoustical Experiment

4.1. Planar Interfaces

[19] The first experiment we present concerns the wavelet response of plates with finite thicknesses and is aimed at experimentally reproducing the synthetic examples presented above. From a geological point of view, these experiments could, for instance, correspond to the remote probing of an open fracture.

4.1.1. Experimental wavelet response

[20] We now present an experimental application of the wavelet response presented in sections 3.1–3.3. The main components of the experimental setup are shown in Figure 7. The wavelet response could in principle be obtained by deconvolving the reflected waves produced by a broadband source signal. However, both nonlinearities of the apparatus and numerical instabilities produced by noise make this method too inaccurate. In practice, we observed that much more accurate signals are obtained by using exact source wavelets. This is practically implemented by searching for the input numerical signals sent to the arbitrary waveform generator such that the output signals recorded with the receiving transducer are an imposed wavelet family. This is performed through a nonlinear inverse method based on

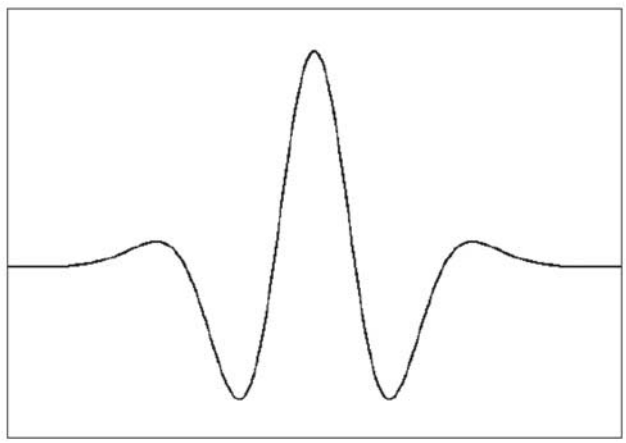

Figure 8. The analytical wavelet used for the experiments is the fourth derivative of a Gaussian: $d^4/dt^4 e^{-t^2}$.

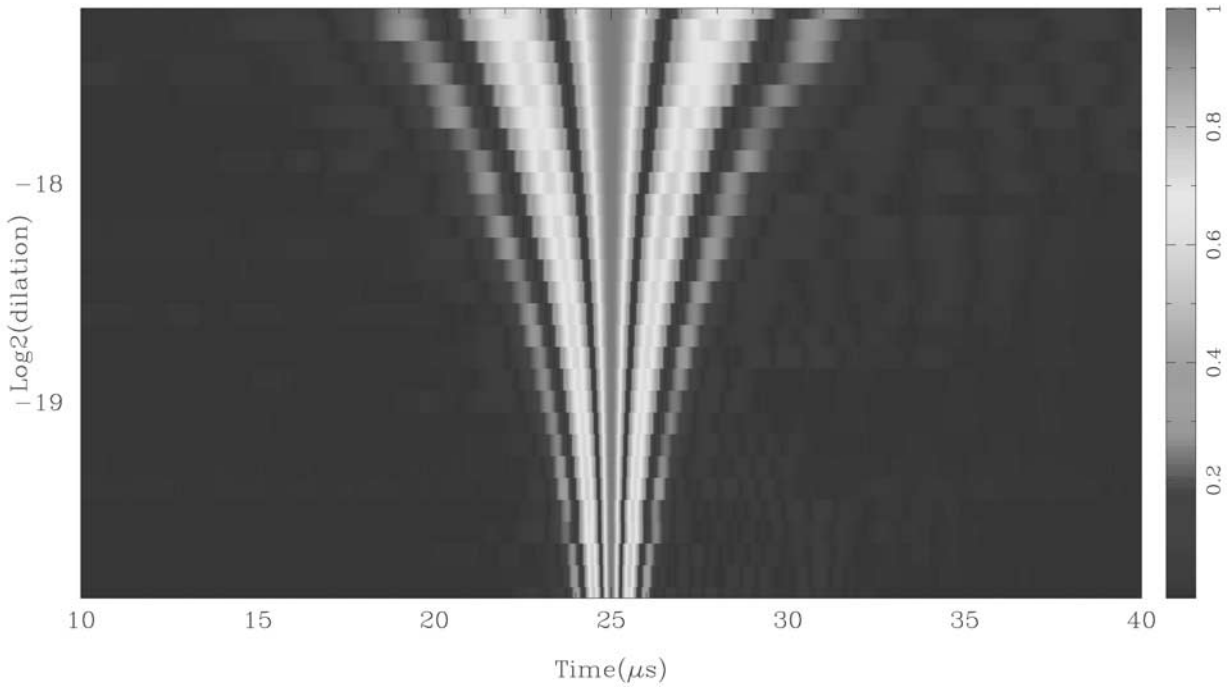

Figure 9. Representation of the modulus of a wavelet response obtained by propagating the source signals through water. The dilation $a = f_c^{-1}$, where f_c is the main frequency of the wavelets which are dilated versions of the fourth derivative of a Gaussian.

simulated annealing and neural network (F. Conil, personal communication, 2002). In the present instance, the analyzing wavelet is the fourth derivative of a Gaussian (Figure 8). Following this procedure, a family of input signals was constructed for four pairs of transducers with central frequencies f_c = 250, 500, 750, and 1000 kHz. For convenience, the output wavelets are such that the dilation $a = f_c^{-1}$, where the central frequency with maximum energy f_c is given in hertz. Figure 9 shows the so obtained wavelet family. The main advantage of this method is that no deconvolution of the data is further needed and this ensures an accurate control of the output signals amplitude for further comparison with reflectivity modeling. Another advantage is that once the input signals are found, the wavelet responses are obtained in real time. This allows for both an immediate control of the quality of the data and an assessment of the signal-to-noise ratio.

[21] The experimental setup consists in a rigid frame holding a pairs of ultrasonic transducers and the target to be analyzed (Figure 10). The targets are polycarbonate plates with thicknesses of 1, 2, 4, and 8 mm. By combining the available frequencies (150 kHz to 1.2 MHz) and plate thicknesses and by appropriately rescaling the data, it is possible to merge the data in order to span five dilation octaves in the wavelet response.

4.1.2. Results and Discussion

[22] Once the wavelet family is constructed (28 wavelets for this experiment), the wavelet response is immediately obtained by emitting the wavelets with the apparatus shown in Figure 10 and by stacking the received signals to directly construct the wavelet response shown in Figure 11a in its noncausal form. The experimental wavelet response appears like the synthetic wavelet response of a window function (Figure 6a) with a single conical pattern at large dilations and two small cones pointing toward the faces of the plate at small dilations. The experimental ridge functions (Figure 11b) have a flat horizontal part at small dilations typical of an Heaviside distribution. At intermediate dilations the ridge functions are wiggly because of complicated interferences occurring inside the reflector (i.e., the plate). The critical dilation $a_c = 2^{-19}$ where this part of the ridge functions begins is an indicator of the thickness of the reflector. Indeed, in the present experiment the wavelet with dilation a_c has a wavelength λ_c = 4.2 mm inside the polycarbonate; that is, λ_c is about twice the thickness of the plate. At large dilations $a > 2^{-17.5}$ the ridge functions again become linear with a negative slope $\alpha \simeq -0.6$, indicating that at large scales the reflector has a Dirac-like appearance. A numerical wavelet response done with the same parameters as those of the water tank experiment produces ridge functions in very good accordance with the experimental ones (Figure 11c).

4.2. Granular Media

[23] In this experiment we analyze the average wavelet response of the complex interface separating an homogeneous medium (i.e., water) and a heterogeneous medium made of glass beads where multiple scattering may produce a strong frequency-dependent attenuation at macroscopic scales [*Sheng*, 1995]. From a geological point of view this experiment corresponds to the remote probing either of the seafloor or of a highly fractured volume of rocks embedded in an otherwise homogeneous medium.

4.2.1. Experimental setup and measurement procedure

[24] The experimental setup is identical to the one used in the previous experiment (Figure 10), excepted that the

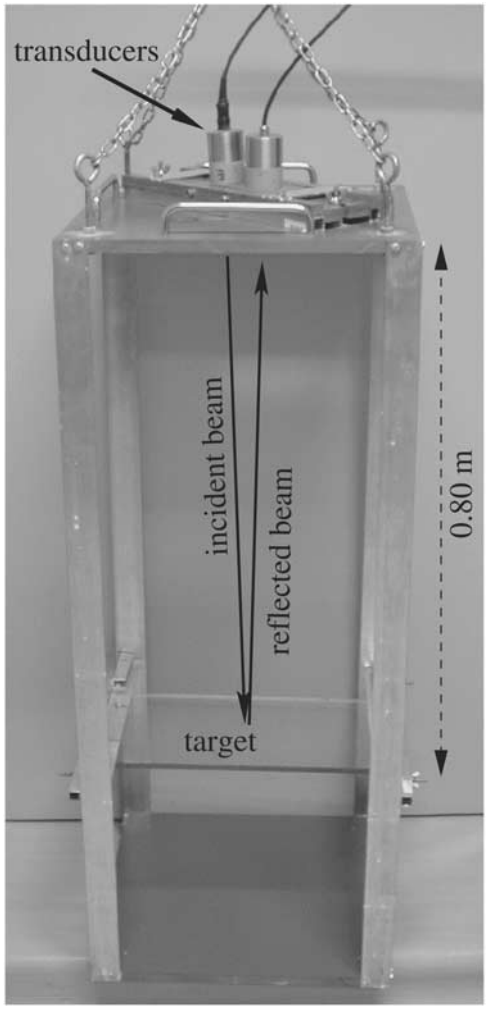

Figure 10. Experimental setup used to perform multiscale ultrasonic probings. The whole apparatus is immersed in a large water tank. Four pairs of transducers are used to span a frequency range from 150 kHz to 1.2 MHz. They are tilted in order to align their beams on a common incident spot. The targets are polyacrylate plates with thicknesses of 1, 2, 4, and 8 mm.

target is now a rolling box filled with glass beads (Figure 12). The average wavelet response is obtained by moving the box and by averaging the individual signals reflected by layer of beads. Since the available four pairs of piezoelectric transducers cover only three frequency octaves, we artificially span the dilation range by merging the results of experiments done with quasi-monodisperse glass bead diameters D = 0.6, 1.1, 2.0, 3.0, 4.0, and 5.0 mm. In this way, 57 relative dilations (i.e., central frequencies between 100 kHz and 5 MHz) are available to construct a common wavelet response (Figure 13) rescaled for the D = 1.1 mm glass beads. For convenience, the dilation is scaled such that $a = \lambda$, where λ is the central wavelength in water.

4.2.2. Results and Discussion

[25] The experimental wavelet response (Figure 13) presents a single global conical appearance at large dilations that splits into several subconical features at medium dilations before being very complex in the small-dilation domain. Several ridge functions spanning the whole dilation range have been extracted and are shown in a log-log diagram in Figure 14. The curves are constituted by five main parts, related to very different acoustic wave behaviors. The flat slope $\alpha = 0$ observed at large dilations $a = \lambda > 2\pi D$ (region V in Figure 14) indicates that the heterogeneous medium is perceived as an homogeneous nonattenuating effective medium with a sharp Heaviside-like surface. Indeed, the reflectivity corresponding to the level of the horizontal segment in dilation band V accurately agrees with the reflectivity predicted by both the *Kuster and Toksöz* [1974] and the *Berryman* [1980] models of effective medium for granular media. The small-dilation end of band V marking the transition between bands IV and V is sharp and corresponds to a wavelength $\lambda = 2\pi D$. The corresponding dilation a then precisely indicates where the quasi-static effective medium models cease to correctly represent the physical system and should be replaced by more sophisticated ones [e.g., *Waterman and Truell*, 1961].

[26] Dilation bands IV, III, and II correspond both to increasing wave scattering effects and to different scattering regimes, respectively. Both bands II and IV correspond to almost straight ridge segments with slopes $\alpha = 2$ and $\alpha = 1.$, respectively. As in band V, backscattering remains dominant in band IV but with a much larger scattering cross section. However, the conical pattern in dilation range IV looks similar to the one in band V and corresponds to a well-identified interface. Forward scattering becomes dominant in band II where the conical pattern begins to split and is blurred by the coda. Band III corresponds to a regime where transverse scattering is dominant. So, a large part of the acoustic energy is scattered in directions perpendicular to the incident beam, and this results in a decrease of the reflectivity. Finally, in the small-dilation band I the average slope is again $\alpha \simeq 0$ and corresponds to reflection of high-frequency waves onto the irregular surface made by the shallowest layer of glass beads. Hence, in this band, the medium is perceived an homogeneous one (i.e., glass) with a rough surface. The roughness of the surface produces the scattering of the reflectivity with respect to the average horizontal level.

5. Conclusion

[27] We have shown how the wavelet transform can be used to identify and characterize abrupt changes present in a signal. These abrupt changes produce conspicuous cone-like patterns in the wavelet transform with their apex pointing toward the homogeneity centers of the singularities. A local analysis of each abrupt change is possible by using the ridge functions extracted from the modulus of the wavelet transform. The global appearance of multiscale clusters of abrupt changes is characterized in the large-dilation domain $a > a_c$ by the slope α of the ridge functions which appear almost straight when plotted in a log-log diagram. At these global scales an interface may be considered as a single abrupt change with regularity α. At finer dilations $a < a_c$ the ridge functions cease to be straight, and the interface may no more be considered as a single feature but instead must be seen as a cluster of small-scale features with their own cone-like pattern in the wavelet

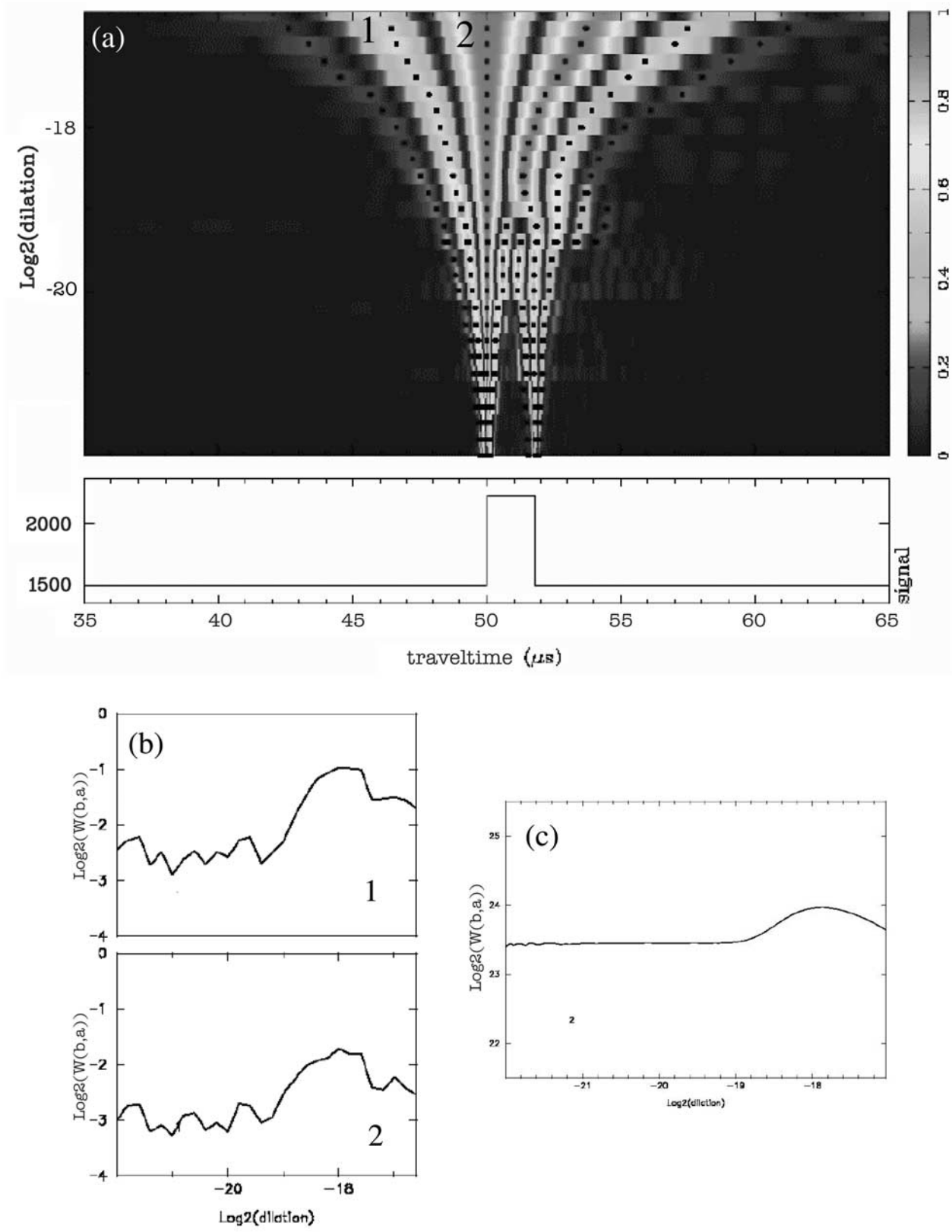

Figure 11. (a) Modulus of the experimental wavelet response of a polycarbonate plate immersed in water. At large dilations the wavelet response resembles that of a Dirac distribution, while at small dilations, two cones point toward the faces of the plate and count one less ridge function. (b) The $\log_2$-$\log_2$ plot of two ridge functions of the wavelet response displayed in Figure 11a. (c) Synthetic ridge function obtained by performing a 1D numerical wavelet response with parameters identical to those of the water tank experiment.

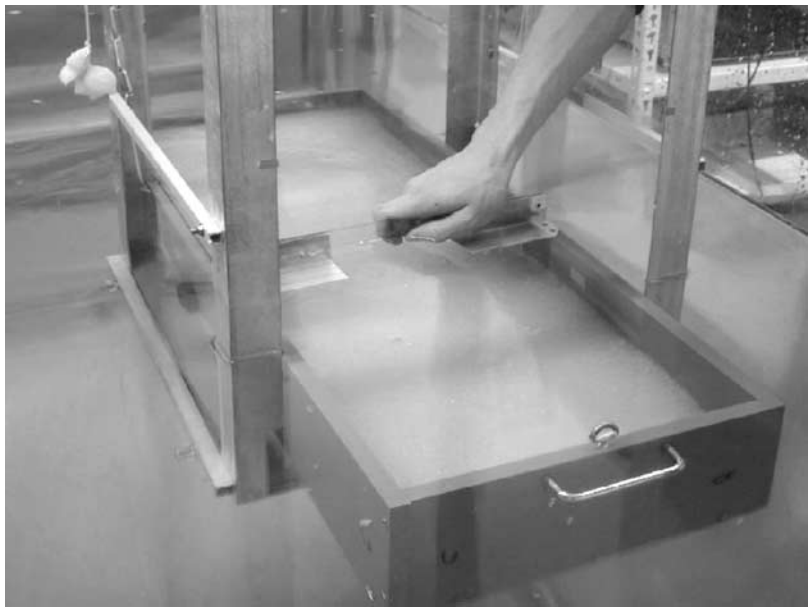

Figure 12. The surface of the granular medium constituted by glass beads is manually smoothed by translating a Plexiglas slab held vertically across the box. Two passes with the slab are sufficient to suppress surface irregularities larger than one bead diameter while avoiding any regular arrangement in the shallowest layers of beads.

transform. Despite complicated interference phenomena among the individual cones generally which preclude an analysis of each small-scale event, the overall size of the cluster may be estimated from the corner dilation a_c at which the large-scale behavior of the interface ceases to hold.

[28] The wavelet response is a natural extension of the wavelet transform when the signal to be analyzed (i.e., the

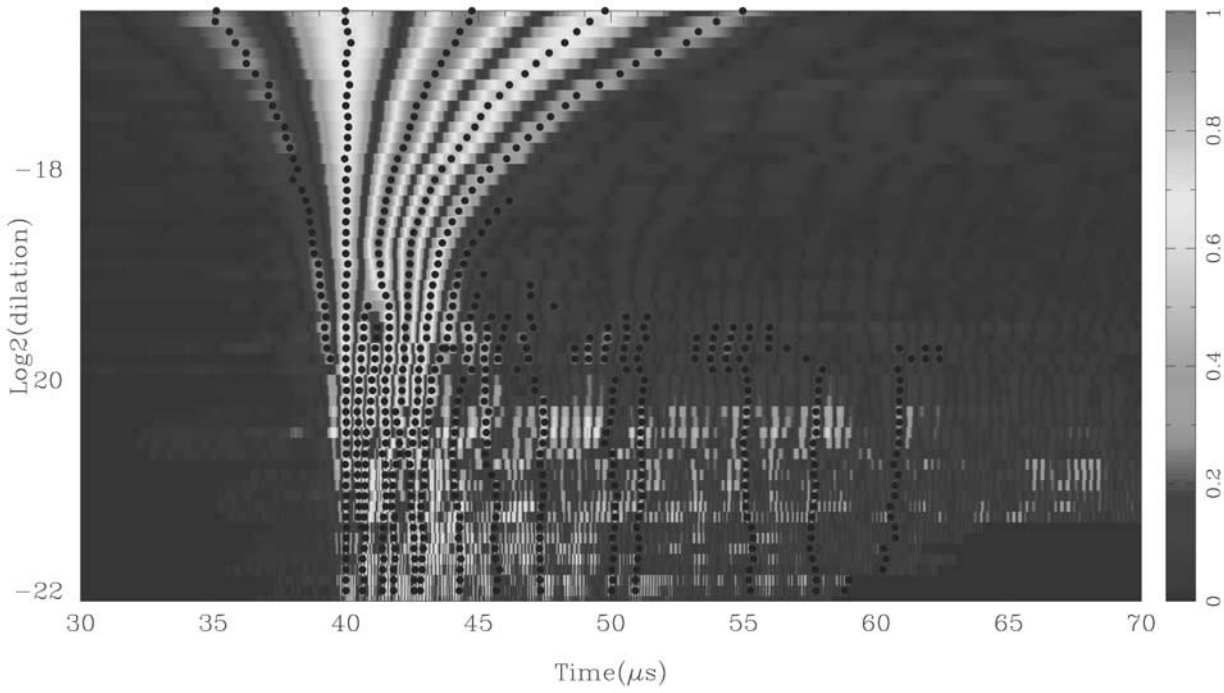

Figure 13. Modulus of the experimental wavelet response rescaled for glass beads with $d = 1.1$ mm (see text for details). The black dots represent the lines of maxima associated with the ridge functions shown as symbols in Figure 14. The individual signals forming this noncausal wavelet response have been arbitrarily shifted in time in order to align their second relative maxima (dotted line of maxima labeled 1).

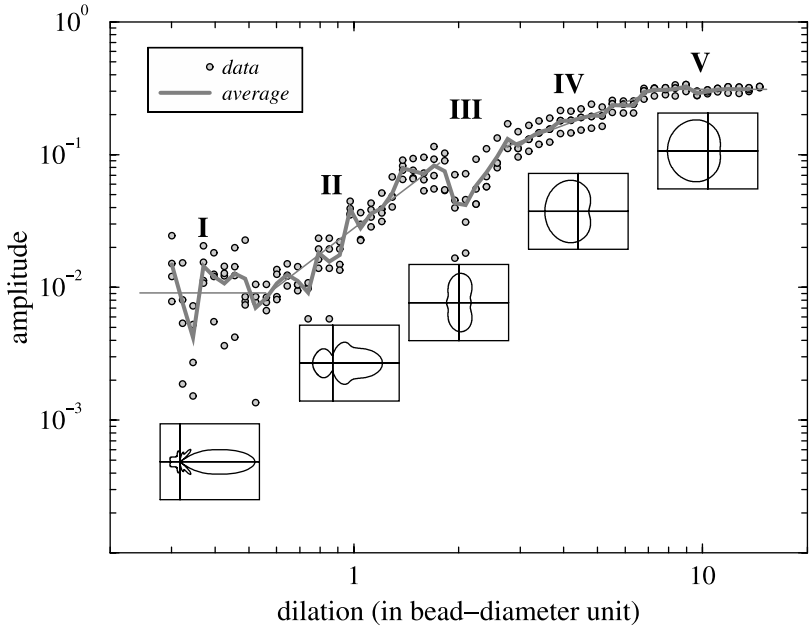

Figure 14. Experimental ridge functions (symbols) corresponding to the labeled lines of maxima extracted from the experimental wavelet response shown in Figure 13 and plotted in a log-log diagram. The average ridge function (solid line) is mostly linear in four dilation bands represented by the straight segments with slopes equal to 0, +2, +1, and 0 for the dilation bands I, II, IV, and V, respectively. The insets show the Mie scattering amplitude $|f(\theta)|$ of a single glass bead for each dilation band.

velocity profile of the medium) cannot be directly convolved with the wavelets but can only be remotely probed by propagating wavelets into the medium. The reflected waves produced by the impinging of the incident wavelets onto the interfaces present in the medium constitute the wavelet response. We have shown that both transforms are essentially equivalent when multiple scattering is neglected. As for the wavelet transform, cone-like features and ridge functions can be recognized in the wavelet response, and applications of the wavelet response reveal that useful information can be obtained about complex interfaces, namely, the large-scale regularity of the single equivalent interface and the size of the cluster of the small-scale variations forming the global interface. Surprisingly, the wavelet response can be analyzed over a narrower dilation range than the one necessary in the wavelet transform (4 octaves against 6). Thanks to numerically controlled piezoelectric transducers, a family of wavelet sources can be directly emitted by the experimental setup in order to probe a reflector in real time. The experimental results obtained for targets made with polycarbonate plates totally agree with the numerical examples and give an insight on how to design and build sounding devices able to characterize remote targets. An experiment done with a complex interface corresponding to the top of a layer of glass beads immersed in water shows that the wavelet response allows determination of the wavelength band where the interface may be replaced as Heaviside-like with a reflectivity given by a quasi-static elastic effective medium.

[29] **Acknowledgments.** We thank Gwennan Carel for her collaboration during the preliminary steps of this study. Frédéric Conil and Michel Lemoine helped us in designing the experimental setup. This work is financially supported by the CNRS and ANDRA through the GdR FORPRO (Research action 99.II) and corresponds to GdR FORPRO contribution 2000/32A.

References

Alexandrescu, M., D. Gibert, G. Hulot, J.-L. Le Mouël, and G. Saracco, Detection of geomagnetic jerks using wavelet analysis, *J. Geophys. Res.*, *100*, 12,557–12,572, 1995.

Alexandrescu, M., D. Gibert, G. Hulot, J.-L. Le Mouël, and G. Saracco, Worldwide wavelet analysis of geomagnetic jerks, *J. Geophys. Res.*, *101*, 21,975–21,994, 1996.

Argoul, F., A. Arnéodo, G. Grasseau, Y. Gagne, E. J. Hopfinger, and U. Frisch, Wavelet analysis of turbulence reveals the multifractal nature of the Richardson cascade, *Nature*, *338*, 51–53, 1989.

Banik, N. C., I. Lerche, and R. T. Shuey, Stratigraphic filtering, Part 1: Derivation of the O'Doherty–Anstey formula, *Geophysics*, *50*, 2768–2774, 1985.

Berryman, J. G., Long-wavelength propagation in composite elastic media: Spherical inclusions, *J. Acoust. Soc. Am.*, *68*, 1809–1819, 1980.

Bleistein, N., On the imaging of reflectors in the Earth, *Geophysics*, *52*, 931–942, 1987.

Burridge, B., G. Papanicolaou, and B. White, One-dimensional wave propagation in a highly discontinuous medium, *Wave Motion*, *10*, 19–44, 1988.

Claerbout, J. F., *Fundamentals of Geophysical Data Processing*, McGraw-Hill, New York, 1976.

Dobrin, M. B., *Introduction to Geophysical Prospecting*, 4th ed., McGraw-Hill, New York, 1988.

Gibson, B. S., and A. R. Levander, Apparent layering in common-midpoint stacked images of two-dimensionally heterogeneous targets, *Geophysics*, *55*, 1466–1477, 1990.

Goupillaud, P., A. Grossmann, and J. Morlet, Cycle-octave and related transforms in seismic signal analysis, *Geoexploration*, *23*, 85–102, 1984.

Gray, S. H., and N. Bleistein, Imaging and inversion of zero-offset seismic data, *Proc. IEEE*, *74*, 440–456, 1986.

Grossmann, A., Wavelet transform and edge detection, in *Stochastic Processes in Physics and Engineering*, edited by M. Hazewinkel, pp. 149–157, D. Reidel, Norwell, Mass., 1986.

Grossmann, A., and J. Morlet, Decomposition of Hardy functions into square integrable wavelets of constant shape, *SIAM J. Math. Anal.*, *15*, 723–736, 1984.

Grossmann, A., M. Holschneider, R. Kronland-Martinet, J. Morlet, Detection of abrupt changes in sound signals with the help of wavelet trans-

forms, in *Inverse Problems: An Interdisciplinary Study*, *Adv. Electr. Electr. Phys., Suppl. 19*, pp. 298–306, Academic, San Diego, Calif., 1987.

Henry, G., *La Sismique Réflexion: Principes et Développements*, Technip, Paris, 1997.

Herrmann, F. J., Scaling of the pseudo primary analyzed by the wavelet transform, paper presented at 64th Meeting, Soc. of Explor. Geophys., Tulsa, Okla., 1994.

Herrmann, F. J., and J. J. Staal, Waves in scaling media, the implication of non-differentiability, in *58th Annual EAGE Conference*, edited by D. J. Feenstra, Abstract C007, Eur. Assoc. of Geosci. and Eng., Amsterdam, 1996.

Holschneider, M., *Wavelets: An Analysis Tool*, 423 pp., Clarendon, Oxford, England, 1995.

Knapp, R. W., Vertical resolution of thick beds, thin beds, and thin-bed cyclothems, *Geophysics*, *55*, 1183–1190, 1990.

Kuster, G. T., and M. N. Toksöz, Velocity and attenuation of seismic waves in two-phase media: Theoretical formulation, *Geophysics*, *39*, 587–618, 1974.

Mallat, S., and W. L. Hwang, Singularity detection and processing with wavelets, *IEEE Trans. Inf. Theory*, *38*, 617–643, 1992.

Marsan, D., and C. J. Bean, Multiscaling nature of sonic velocities and lithology in the upper crystalline crust: Evidence from the KTB main borehole, *Geophys. Res. Lett.*, *26*, 275–278, 1999.

Scales, J. A., On the use of localization theory to characterize elastic wave propagation in randomly stratified 1-D media, *Geophysics*, *58*, 177–179, 1993.

Sheng, P., *Introduction to Wave Scattering, Localization and Mesoscopic Phenomena*, Academic, San Diego, Calif., 1995.

Sheng, P., Z. Q. Zhang, B. White, and G. Papanicolaou, Multiple-scattering noise in one dimension: Universality through localization-length scaling, *Phys. Rev. Lett.*, *57*, 1000–1003, 1986.

Sheng, P., B. White, and B. Nair, Lithological correlations and seismic wave localisation in the Earth's subsurface, *Inverse Problems*, *5*, 57–63, 1989.

Walden, A. T., and J. W. J. Hosken, The nature of the non-Gaussianity of primary reflection coefficients and its significance for deconvolution, *Geophys. Prospect.*, *34*, 1038–1066, 1986.

Wapenaar, K., Seismic reflection and transmission coefficients of a self-similar interface, *Geophys. J. Int.*, *135*, 585–594, 1998.

Wapenaar, K., Amplitude-variation-with-angle behavior of self-similar interface, *Geophysics*, *64*, 1928–1938, 1999.

Waterman, P. C., and R. Truell, Multiple scattering of waves, *J. Math. Phys.*, *2*, 512–537, 1961.

Widess, M. A., How thin is a thin bed?, *Geophysics*, *38*, 1176–1180, 1973.

Widess, M. A., Quantifying resolving power of seismic systems, *Geophysics*, *47*, 1160–1173, 1982.

D. Gibert, Y. Le Gonidec, and J.-N. Proust, Géosciences Rennes, Université Rennes 1, B15 Campus de Beaulieu, F-35042 Rennes cedex, France. (gibert@univ-rennes1.fr; ylegonid@univ-rennes1.fr; jean-noel.proust@univ-rennes1.fr)